LETTER • **OPEN ACCESS**

Ballistic graphene-$NbSe_2$ Josephson junction in high parallel magnetic field

To cite this article: Einav Grynszpan *et al* 2025 *2D Mater.* **12** 041004

2D Materials

OPEN ACCESS

RECEIVED
6 April 2025

REVISED
1 September 2025

ACCEPTED FOR PUBLICATION
17 September 2025

PUBLISHED
22 October 2025

LETTER

Ballistic graphene-$NbSe_2$ Josephson junction in high parallel magnetic field

Einav Grynszpan[1], Ayelet Zalic[1], Pradheesh Ramachandran[1], Takashi Taniguchi[2], Kenji Watanabe[3], Anna Keselman[4,5] and Hadar Steinberg[1,6,*]

[1] The Racah Institute of Physics, The Hebrew University of Jerusalem, Jerusalem 91904, Israel
[2] International Center for Materials Nanoarchitectonics, National Institute for Materials Science, 1-1 Namiki, Tsukuba 305-0044, Japan
[3] Research Center for Functional Materials, National Institute for Materials Science, 1-1 Namiki, Tsukuba 305-0044, Japan
[4] Physics Department, Technion—Israel Institute of Technology, Haifa 32000, Israel
[5] The Helen Diller Quantum Center, Technion, Haifa 32000, Israel
[6] The Center for Nanoscience and Nanotechnology, The Hebrew University of Jerusalem, Jerusalem 91904, Israel
[*] Author to whom any correspondence should be addressed.

E-mail: hadar@phys.huji.ac.il

Keywords: superconductivity, graphene, $NbSe_2$, TMD, Josephson effect, ballistic, Josephson junction

Supplementary material for this article is available online

Abstract

Planar graphene-$NbSe_2$ Josephson junctions can support supercurrents at high in-plane magnetic fields ($B_{||}$) due to the robust superconductivity in thin $NbSe_2$, protected from both orbital and spin-driven decay by a combination of atomic thickness and Ising spin orbit coupling. We fabricate and characterize a clean, flat graphene-$NbSe_2$ junction encapsulated in hBN. The junction is ballistic, exhibiting Fabry–Pérot oscillations of the critical current, and supports very high critical current densities. The junction is remarkably robust to both in-plane and out-of-plane magnetic fields, and exhibits a clear ballistic Josephson effect up to the maximally available in-plane field of 8 T. We model the suppression of the critical current using a tight-binding model, accounting for the large overlap area between the $NbSe_2$ and graphene. We find that the suppression is governed by both the Zeeman splitting of Andreev bound states and by the flux threading the van-der-Waals gap that separates graphene from the $NbSe_2$ leads.

In recent years, there has been growing interest in lateral Josephson junctions (JJs) configured in a planar geometry. These junctions serve as platforms for exploiting material transport properties that arise from geometry and proximity effects, to induce phenomena that are not inherent to the superconductor alone. Like in JJs based on ferromagnetic weak links [1], junction weak links can generate Cooper pairs with a non-zero center-of-mass momentum when a parallel magnetic field, $B_{||}$, is applied in the junction plane [2–5]. When materials that permit the presence of spin–orbit coupling in the weak link are used in the JJ architecture, the system can be driven to non-trivial topological states [2, 6].

An example of such systems are graphene-based JJs, which came to prominence in 2007 [7] and provide a promising new platform to study surface-addressable high-quality 2D systems coupled to superconductors [8]. The first ballistic graphene JJs utilized suspended graphene [9], while today they are more readily constructed from graphene encapsulated by hexagonal boron nitride (hBN), with superconducting side contacts [10–12]. A hallmark of these junctions are the observed Fabry-Pérot oscillations in the critical current (I_C), which serve as evidence of ballistic superconductivity [11, 13].

Owing to its low-disorder interface with graphene, $NbSe_2$ presents itself as a compelling material choice for integration into graphene-based devices, especially those designed to function in high magnetic fields. This is bolstered by the fact that thin layers of $NbSe_2$ remain superconducting at very high fields due to a combination of Ising protection [14] and suppressed orbital depairing [15–17]. Recently, devices of this kind have been realized with the successful fabrication of van der

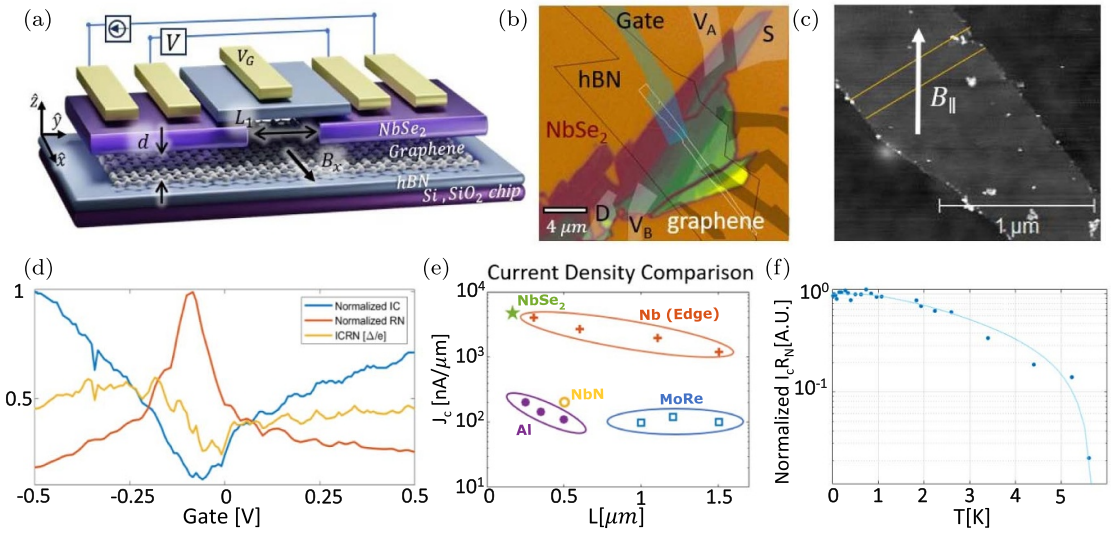

Figure 1. Device characterization. (a) Schematic of $NbSe_2$-graphene Josephson junction device, encapsulated in hBN. The device has four contact electrodes and a top gate electrode. (b) Microscope image of the cracked $NbSe_2$, with the outlines of top hBN (graphene) flakes shown in black (white) and the contact electrodes shown in false color. (c) AFM measurement of graphene flake after transfer to hBN substrate, heat cleaning and tip cleaning. The location of the subsequently transferred $NbSe_2$ crack is shown between yellow lines, while the in-plane orientation of $B_\parallel$ is shown by the white arrow. (d) Critical current I_C, normal resistance R_N and calculated I_CR_N product as a function of gate voltage. All traces exhibit Fabry Perot oscillations on the electron side. (e) Current densities for graphene JJs, based on the compilation in [22] (Nb side contacts) with data taken from [9] (suspended graphene with NbN contacts) [10], (MoRe side contacts) [13] (Al contacts). The device reported here is marked by a star. (f) Normalized I_CR_N as a function of temperature. The solid line is the result of a tight-binding calculation, assuming a value of $\Delta^* = 0.6$ meV for the induced gap in graphene.

Waals Josephson devices that incorporate graphene weak links and $NbSe_2$ contacts, which we will refer to as two-dimensional Josephson junctions (2DJJs) [18, 19]. In previous experiments involving these devices, we have explored diffusive 2DJJs and SQUID devices at high $B_{||}$, observing possible signatures of field-driven finite-momentum Cooper pairing, as well as current density redistribution within the graphene weak link [19, 20].

In this letter we present evidence of an all-vdW lateral ballistic 2DJJ. The device exhibits gate-driven Fabry–Pérot oscillations, which manifest both in the normal resistance R_N and in the critical current I_C. The device is robust to magnetic field directed both in ($B_\parallel$) and out ($B_\perp$) of the plane of the junction—sustaining a finite critical current at $B_\perp$ reaching close to 1 T out of plane, and $B_\parallel = 8$ T. In the latter case we find a suppression of 2 orders of magnitude in the critical current. To explain the observed I_C suppression, we develop a tight-binding model which accounts for both the Zeeman splitting and the orbital effect of the graphene-$NbSe_2$ vdW gap. The interlayer spacing, although only 0.52 nm wide [21], appears to have a decisive effect on the suppression of supercurrent at the high $B_\parallel$ limit.

We fabricate the device using a cracked flake of $NbSe_2$ placed on a graphene ribbon, fully encapsulated by hBN from both the top and bottom (see illustration in figure 1(a) and microscope image of the device shown in figure 1(b)). The $NbSe_2$ flake is contacted on either side of the crack by evaporated Ti-Au electrodes in a four-probe geometry. The $NbSe_2$ crack length in the direction of the current flow measures approximately $L_1 \approx 160$ nm, while the underlying graphene ribbon has a width of $W \approx 1$ μm and a length of $L_2 \approx 9$ μm beneath the $NbSe_2$ contacts. The $NbSe_2$ in the vicinity of the crack is only about 3–5 layers thick (evaluated by optical contrast). At such thicknesses, the superconducting gap is measurably reduced, down to 0.75–1 meV, in comparison with the bulk gap of 1.2 meV. Ising spin–orbit coupling has an appreciable effect on the retention of the gap at high in-plane magnetic fields [16, 23]. The graphene carrier density is adjusted via a top gate electrode that is insulated from the device by the top hBN flake, which is 11 nm thick, as shown in figures 1(a) and (b).

We begin our characterization by exploring the critical current as a function of the gate voltage, shown in figure 1(d). I_C and R_N exhibit Fabry–Pérot oscillations at electron doping, indicating ballistic supercurrent transport in a cavity [10–13]. Both modulate with gate voltage such that their product maintains constant, $I_CR_N \approx 0.5\Delta/e$ away from the Dirac point. This is smaller than the theoretically expected proportionality constant of $2.44\Delta/e$ for short ballistic graphene JJ [24]. However, experimental observations show values near $2\Delta/e$ in

Al-contact junctions [25], and in ballistic graphene junctions this constant has been found to be even smaller [26].

The F-P oscillations are most pronounced on the electron side, $V_G > 0$, and are a consequence of the formation of PN junctions between the n-doped graphene between the $NbSe_2$ leads, and the strongly p-doped graphene underneath them. From the periodicity of the FP oscillations, $2k_F L_{FP}$, we extract the length of the P-N-P cavity $L_{FP} \approx 150$ nm.

The resulting $NbSe_2$-graphene contacts have a transparency of ≈0.82 for $V_G = -0.5$ V (hole doping), and ≈0.6 for $V_G = 0.5$ V (electron doping), calculated following [11] (see supplementary section 1 for details). Transparency is lower on the electron side due to the formation of P-N junctions. On the hole side, transparency might be limited by the p-p' junctions formed as a result of higher hole doping within the contact region.

The highly transparent contact yields a large critical current density of ≈4000 nA μm^{-1} at $V_G = -1$ V, comparable to state-of-the-art Nb edge contacts [22] (see figure 1(e)). This device is nominally in the ballistic short junction regime, with the Thouless energy $E_{Th} = \hbar v_F / L_1 \approx 4$ meV [11], a few times larger than the superconducting gap ($\Delta = 1.2$ mV for bulk $NbSe_2$ and smaller for thin $NbSe_2$). In figure 1(f) we show the normalized temperature dependence of the $I_C R_N$ product.

The junction remains superconducting up to 5.5 K, not far below the T_C of 3–4 layer $NbSe_2$. The Josephson effect in our junction is retained in both in-plane and out-of-plane magnetic fields. To show this, we first turn to transport measurements with magnetic fields applied perpendicular to the plane of the junction. In figure 2(a), we explore the junction differential resistance at zero bias as a function of V_G and magnetic field, up to $B_\perp = 2.7$ T. The device exhibits two main features: At high fields, transport is normal, with a Landau fan typical of the quantum Hall regime measured in a 2-terminal geometry. At lower fields, superconductivity is observed below the white curves marked in the figure. These curves indicate the limit of the semiclassical regime given by $r_C = L$, where r_C is the cyclotron radius. There are even hints of superconductivity well into the quantum Hall regime (see supplementary section 2).

At the mT limit the junction is unstable. Unlike the Fraunhofer interference pattern usually observed in JJs, including $NbSe_2$-graphene JJs we reported in earlier studies [19, 20], here we observe a periodic saw-tooth pattern consisting of four lobes of ≈400 μT, shown in figure 2(b). This measurement was taken at $V_G = -0.25$ V. We believe that these jumps are associated with vortices which enter the $NbSe_2$ flakes far from the junction. Individual vortices are expected to have an outsized effect at the ultra-thin limit, where the vortex-induced current-redistribution is governed by the Pearl length scale. The Pearl length is $\Lambda = 2\lambda_L^2/d$, where λ is the London penetration length, and d is the flake thickness. At the present case, the current maps extends over the size of the entire flake.

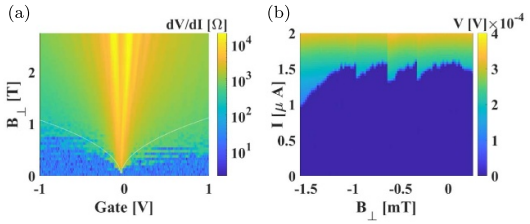

Figure 2. Perpendicular magnetic field. (a) Landau Fan measurement of the differential resistance at zero bias voltage, as a function of $B_\perp$ and V_G. The device exhibits quantum Hall conductance above 1.5 T. Superconductivity survives in most of the semi-classical regime $L < r_C$ (boundary shown in white). (b) $I_C(B_\perp)$ at low fields exhibits discrete jumps in I_C at flux in multiples of ≈ 400 μT, likely associated with remote vortices. This dataset was taken at $V_G = -0.25$ V.

We now turn to the measurements in parallel magnetic field $B_{||}$, which constitute the main results of this work. Figure 3(a) shows maps of junction voltage vs. applied current and V_G. The measurement is repeated at several values of $B_{||}$. At each value of $B_{||}$, we compensate $B_\perp$ to reach a maximal critical current [19, 20]. We note that this can be done even considering the vortex instability described above. The leftmost scan, corresponding to $B_{||} = 0$ extends the data shown in figure 1(d). At $B_{||} = 0$ T hole carriers had a larger critical current, as explained by the higher transparency of the channel in the absence of a P-N-P junction. Remarkably, as we increase $B_{||}$ we continue to observe FP oscillations at all fields in the range accessible to our magnet, up to 8 T. However, the magnitude of I_C decays from the μA scale at zero field, to the order of 10nA at $B_{||} = 8$T. This result confirms the retention of superconducting ballistic transport at these high fields. The periodicity of the oscillations remains consistent and their visibility even increases.

In figure 3(b) we plot $I_C(B_{||})$, measured at $V_G = -0.4$ V while tracking I_C decay. The exact mechanism leading to this decay is not obvious, and is the focus of the remaining part of this work. In what follows, we discuss three possible mechanisms for critical current suppression: (i) Suppression of the $NbSe_2$ superconducting gap Δ; (ii) The effect of Zeeman splitting of the Andreev bound states (ABS) and (iii) Threading magnetic flux through the vdW gap between the $NbSe_2$ and graphene.

Considering the first mechanism, involving the effect of Δ, it is well known that in thin $NbSe_2$ the gap remains stable well above 10 T [15]. We can rule

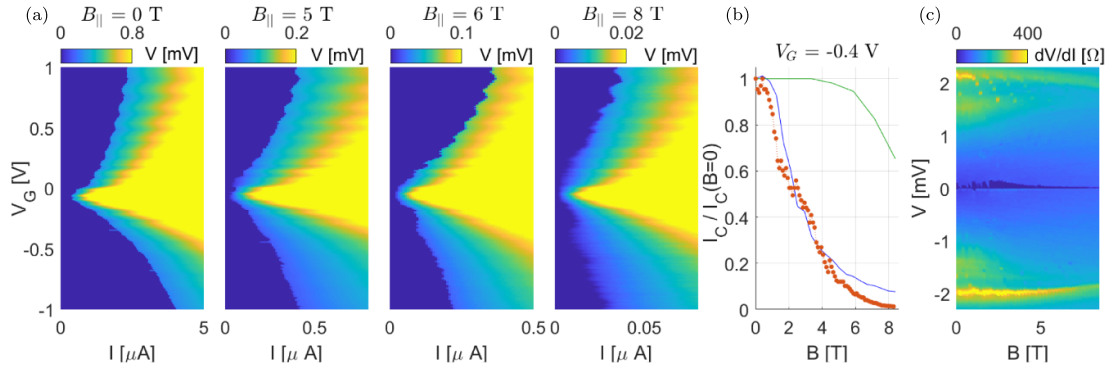

Figure 3. (a) Junction voltage as a function of current and V_G at different values of in-plane magnetic field. The boundary between 0 and finite voltage regions indicates the critical current. The data exhibits Fabry Pérot oscillations of both I_C and R_N, shown here at selected values of $B_{||} = 0$ T, 5 T, 6 T, and 8 T (from left to right). (b) Critical current decay vs. $B_{||}$. Data in orange. Blue and green solid lines are tight-binding calculations, assuming induced gap of $\Delta^* = 0.6$ meV, with and without the effect of flux threading respectively (further details on the tight-binding model are given in the supplementary material section S2.2). (c) Differential resistance vs. bias voltage and $B_{||}$. Andreev reflection peaks hardly change their voltage as a function of $B_{||}$, confirming that the field has only a small effect on the superconducting gap.

out the role of Δ in suppressing I_C in our device by measuring the differential resistance as a function of bias voltage, shown in figure 3(c) (data taken at large hole doping $V_G = -1.5$ V). The data exhibits a conductance enhancement at low bias and resistance peaks at $\pm 2\Delta$, as expected for Andreev reflection. Multiple Andreev reflection features at sub-gap energies $2\Delta/n$ are not detected. The main resistance peak 2.1 meV likely represents 2Δ for the large $NbSe_2$ gap. It is notable that the peak maintains near constant bias voltage as a function of magnetic field, confirming that Δ is hardly affected by the field as expected for thin $NbSe_2$. The origin of the lower energy spectral feature is not clear, and could be related to the induced gap in graphene. The smaller $NbSe_2$ gap, studied in [16] should not be visible at the thin $NbSe_2$ limit.

A second mechanism which would lead to critical current suppression is related to the spin-splitting of the ABS within the junction. However this suppression is only expected when the Zeeman splitting $2E_Z = g\mu_B B$ is of order of the Thouless energy E_{Th}. As mentioned above $E_{\mathrm{Th}} \approx 4$ meV in our device and hence a significant suppression of the current would be expected only at fields of order 35 T. In figure 3(b) we plot the predicted critical current in presence of Zeeman splitting, as obtained using a tight-binding model. As can be clearly seen this effect alone cannot account for the decay of the critical current observed experimentally at fields of order 8 T.

Given that neither Δ nor the Zeeman effect are expected to suppress the critical current, we seek for an alternative mechanism based on the parallel accumulation of flux within the junction, as depicted in figure 4(a) [27]. We know that $NbSe_2$ couples to the graphene channel over an extended overlap area. Assuming the vdW gap is $d = 0.6$ nm wide, and the overlap region is about 1 μm long, the resulting area accumulates a single flux quantum for an in-plane field component $B_x \approx 3.5$ T.

This, in turn, suggests that we cannot disregard the contribution of this flux when calculating the properties of the junction. We therefore develop a theoretical model which accounts for the orbital effect of the in-plane magnetic field on the proximity induced gap (figure 4(a)). The model is based on an effective hexagonal lattice representing the proximitized graphene, with a position-dependent induced gap Δ^*. We use the model to calculate the phase-dependent Andreev spectra. The ground state energy of the junction, E_{GS}, is then obtained by summing over the populated states. To extract the critical current we assume $T = 0$ and use $I_c = \max\left|2e\frac{\mathrm{d}E_{\mathrm{GS}}}{\mathrm{d}\varphi}\right|$. A detailed description of the model appears in supplementary section 3.

In the presence of an in-plane field, an electron tunneling from the $NbSe_2$ to the graphene beneath it acquires a position dependent phase $\phi(x,y) = A_z(x,y)d$, where A_z is the perpendicular component of the vector potential. Hereafter, we use a gauge in which the vector potential is given by $\vec{A} = (0, 0, yB_x - xB_y)$. This in turn leads to a variation of $2\phi(x,y)$ in the phase of the superconducting order parameter. In the short junction limit we can neglect the effect of the phase modulation along x (the direction perpendicular to the current). Thus to capture the orbital effect of the field in the numerical simulation, we introduce a position dependent phase for the superconducting order parameter $\Delta^*(y) = \Delta^* e^{iqy}$, where $q = \frac{2e}{\hbar}B_x d$. We use this model to calculate I_C for realistic system parameters. The results are plotted in figure 3(b). To reach these results, we first extract the ABS spectra, which are shown in figure S2. To clarify the roles of the Zeeman and orbital terms, we show simplified spectra obtained for a short, transparent junction in figures 4(b)–(d). For comparison, panel (b) shows

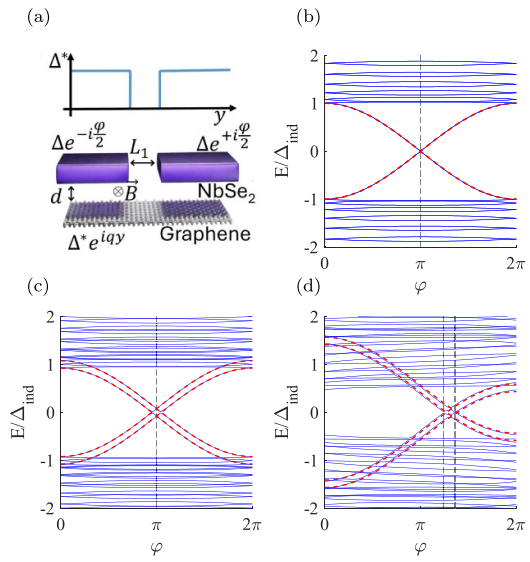

Figure 4. (a) Schematic setup of the junction used in the theoretical modeling. (b)–(d) Simplified energy spectra in the limit of a short perfectly transparent junction obtained using the tight-binding model (see supplementary materials section S4.2) for (b) $B = 0$, (c) $B = 1$T neglecting the orbital effect, i.e. for $d = 0$, here Zeeman splitting of the ABS is clearly seen , and (d) $B = 1$T including both the Zeeman contribution and the orbital effect of the magnetic field as discussed in the text. Note the suppression of the gap and the shift in the crossing of Andreev bound states away from $\varphi = \pi$.

the well-known ABS spectrum for $B = 0$. In panel (c), only the Zeeman coupling is included giving rise to Zeeman split spin-polarized spectra. Importantly, as discussed above and illustrated in figure 3(b), these only give rise to a minimal suppression in I_C, and do not reproduce the current suppression we observe.

To fully reproduce the observed suppression we have to account for both Zeeman and orbital effects. This calculation, shown in figure 4(d), indeed results in a suppressed induced gap, while the ABS crossing shifts away from $\varphi = \pi$. From these spectra we proceed to calculate $I_C(B_\parallel)$, noting that $B_x = B_\parallel \cos(\theta)$, where $\theta = 45°$ (see figure 1(c)). To quantitatively compare the data to the model, we fit for the induced gap Δ^*. In figure S4 we plot the result of the calculation for value of $\Delta^* = 0.4,0.6,0.8$ meV for both the temperature dependence and the magnetic field dependent data. As seen in the figures, the fit successfully reproduces both data-sets at $\Delta^* = 0.6$ meV. $I_C(B_\parallel)$ calculated using the full model, with the above value of Δ^* is shown in figure 3(b), and appears to agree very well with the data.

The 2DJJ reported thus exhibits remarkable stability vs. both in-plane and out-of-plane magnetic field. Specifically, we have shown that the response to in-plane field relies strongly on the nature of the extended contact region between $NbSe_2$ and graphene, and in particular the flux threaded within the atomically thin vdW gap. The role of threaded flux has already been acknowledged in studies involving two dimensional electron systems [27]. Naturally, this problem should not be as severe for the angstrom-scale vdW gaps. However, one should note that recent work on $NbSe_2$ at high parallel fields [28] suggests that the role of the inter-layer flux is highly important in inducing exotic superconducting phases. Finally, our results imply that in order to achieve Josephson devices that do not decay at all with $B_\parallel$, and exhibit pronounced characteristics of 0-π transitions and other spin driven phenomena, it is desirable to limit the extent of the overlap region. Such tests would be addressed in future studies. In conclusion our study reports on an all vdW device with exceptional stability towards applied magnetic fields. Such devices may be useful as part of field-stable quantum architectures. The lack of oxide may make them more stable towards two-level system decoherence—a subject which should be addressed in future studies.

Data availability statement

The data that support the findings of this study are openly available at the following URL/DOI: https://zenodo.org/records/15163380.

Acknowledgments

The authors wish to thank H Dausy, F Pientka, C H Quay and M Aprili for their input. This work was funded by an Israeli Science Foundation Grant 164/23. A Z is grateful to the Azrieli Foundation for Azrieli Fellowships. K W and T T acknowledge support from the Elemental Strategy Initiative conducted by the MEXT, Japan, Grant Number JPMXP0112101001, JSPS KAKENHI Grant Number JP20H00354 and the CREST(JPMJCR15F3), JST. A K acknowledges funding by the Israel Science Foundation (Grant No. 2443/22). Fabrication for this project was carried out at the Harvey Kruger Center for Nano Science and Nano Technology at the Hebrew University.

ORCID iDs

Einav Grynszpan 0000-0002-9420-0315
Kenji Watanabe 0000-0003-3701-8119
Anna Keselman 0000-0002-5226-8522
Hadar Steinberg 0000-0002-7409-5087

References

[1] Buzdin A I 2005 Proximity effects in superconductor-ferromagnet heterostructures *Rev. Mod. Phys.* **77** 935
[2] Pientka F, Keselman A, Berg E, Yacoby A, Stern A and Halperin B I 2017 Topological superconductivity in a planar Josephson junction *Phys. Rev. X* **7** 021032
[3] Hart S, Ren H, Kosowsky M, Ben-Shach G, Leubner P, Brüne C, Buhmann H, Molenkamp L W, Halperin B I and Yacoby A 2016 Controlled finite momentum pairing and spatially varying order parameter in proximitized HgTe quantum wells *Nat. Phys.* **13** 87
[4] Chen A Q, Park M J, Gill S T, Xiao Y, Reig-i Plessis D, MacDougall G J, Gilbert M J and Mason N 2018 Finite

momentum Cooper pairing in three-dimensional topological insulator Josephson junctions *Nat. Commun.* **9** 3478
[5] Holm Fyhn E, Amundsen M, Zalic A, Dvir T, Steinberg H and Linder J 2020 Combined Zeeman and orbital effect on the Josephson effect in rippled graphene *Phys. Rev. B* **102** 024510
[6] Ren H *et al* 2019 Topological superconductivity in a phase-controlled Josephson junction *Nature* **569** 93
[7] Heersche H B, Jarillo-herrero P, Oostinga J B, Vandersypen L M K and Morpurgo A F 2007 Bipolar supercurrent in graphene *Nature* **446** 56
[8] Lee G-H and Lee H-J 2018 Proximity coupling in superconductor-graphene heterostructures *Rep. Prog. Phys.* **81** 056502
[9] Mizuno N, Nielsen B and Du X 2013 Ballistic-like supercurrent in suspended graphene Josephson weak links *Nat. Commun.* **4** 2716
[10] Calado V E, Goswami S, Nanda G, Diez M, Akhmerov A R, Watanabe K, Taniguchi T, Klapwijk T M and Vandersypen L M K 2015 Ballistic Josephson junctions in edge-contacted graphene *Nat. Nanotechnol.* **10** 761
[11] Ben Shalom M *et al* 2016 Quantum oscillations of the critical current and high-field superconducting proximity in ballistic graphene *Nat. Phys.* **12** 318
[12] Amet F *et al* 2016 Supercurrent in the quantum Hall regime *Science* **352** 966
[13] Allen M T *et al* 2017 Observation of electron coherence and Fabry–Perot standing waves at a graphene edge *Nano Lett.* **17** 7380
[14] Xi X, Wang Z, Zhao W, Park J-H, Law K T, Berger H, Forró L, Shan J and Mak K F 2016 Ising pairing in superconducting $NbSe_2$ atomic layers *Nat. Phys.* **12** 139
[15] Kuzmanović M *et al* 2022 Tunneling spectroscopy of few-monolayer $NbSe_2$ in high magnetic fields: triplet superconductivity and Ising protection *Phys. Rev. B* **106** 184514
[16] Dvir T, Massee F, Attias L, Khodas M, Aprili M, Quay C H L and Steinberg H 2018 Spectroscopy of bulk and few-layer superconducting $NbSe_2$ with van der Waals tunnel junctions *Nat. Commun.* **9** 598
[17] de la Barrera S C *et al* 2018 Tuning Ising superconductivity with layer and spin–orbit coupling in two-dimensional transition-metal dichalcogenides *Nat. Commun.* **9** 1427
[18] Lee J, Kim M, Watanabe K, Taniguchi T, Lee G H and Lee H J 2019 Planar graphene Josephson coupling via van der Waals superconducting contacts *Curr. Appl. Phys.* **19** 251
[19] Dvir T, Zalic A, Fyhn E H, Amundsen M, Taniguchi T, Watanabe K, Linder J and Steinberg H 2021 Planar graphene-$NbSe_2$ Josephson junctions in a parallel magnetic field *Phys. Rev. B* **103** 115401
[20] Zalic A, Taniguchi T, Watanabe K, Gazit S and Steinberg H 2022 High magnetic field stability in a planar graphene-$NbSe_2$ squid (arXiv:2211.01020)
[21] Jiang W, Sofer R, Gao X, Kronik L, Hod O, Urbakh M and Ouyang W 2024 Anisotropic interlayer force field for heterogeneous interfaces of graphene and h-BN with transition metal dichalcogenides *J. Phys. Chem. C* **129** 1417
[22] Zhu M, Ben Shalom M, Mishchsenko A, Fal'ko V, Novoselov K and Geim A 2018 Supercurrent and multiple andreev reflections in micrometer-long ballistic graphene Josephson junctions *Nanoscale* **10** 3020
[23] Khestanova E *et al* 2018 Unusual suppression of the superconducting energy gap and critical temperature in atomically thin $NbSe_2$ *Nano Lett.* **18** 2623
[24] Titov M and Beenakker C W J 2006 Josephson effect in ballistic graphene *Phys. Rev. B* **74** 041401
[25] Park J, Lee J H, Lee G-H, Takane Y, Imura K-I, Taniguchi T, Watanabe K and Lee H-J 2018 Short ballistic Josephson coupling in planar graphene junctions with inhomogeneous carrier doping *Phys. Rev. Lett.* **120** 077701
[26] Borzenets I V *et al* 2016 Ballistic graphene Josephson junctions from the short to the long junction regimes *Phys. Rev. Lett.* **117** 237002
[27] Haxell D Z, Coraiola M, Sabonis D, Hinderling M, Ten Kate S C, Cheah E, Krizek F, Schott R, Wegscheider W and Nichele F 2023 Zeeman- and orbital-driven phase shifts in planar Josephson junctions *ACS Nano* **17** 18139
[28] Wan P *et al* 2023 Orbital Fulde–Ferrell–Larkin–Ovchinnikov state in an Ising superconductor *Nature* **619** 46–51
[29] Zomer P J, Guimarães M H D, Brant J C, Tombros N and van Wees B J 2014 Fast pick up technique for high quality heterostructures of bilayer graphene and hexagonal boron nitride *Appl. Phys. Lett.* **105** 013101
[30] Engels S, Terrés B, Klein F, Reichardt S, Goldsche M, Kuhlen S, Watanabe K, Taniguchi T and Stampfer C 2014 Impact of thermal annealing on graphene devices encapsulated in hexagonal boron nitride *Phys. Status Solidi b* **251** 2545
[31] Goossens A M, Calado V E, Barreiro A, Watanabe K, Taniguchi T and Vandersypen L M K 2012 Mechanical cleaning of graphene *Appl. Phys. Lett.* **100** 073110